Gastroenterology 2024;167:547–559

Three-Dimensional Imaging of the Enteric Nervous System in Human Pediatric Colon Reveals New Features of Hirschsprung's Disease

Joshua D. Eisenberg,[1,2] Rebecca P. Bradley,[1] Kahleb D. Graham,[1,3,4] Rachel H. Ceron,[1,5] Amanda M. Lemke,[1] Benjamin J. Wilkins,[6] Ali Naji,[7] and Robert O. Heuckeroth[1,2]

[1]Abramson Research Center, Children's Hospital of Philadelphia Research Institute, Philadelphia, Pennsylvania; [2]Department of Pediatrics, Perelman School of Medicine, University of Pennsylvania, Philadelphia, Pennsylvania; [3]Division of Gastroenterology, Hepatology and Nutrition, Cincinnati Children's Hospital Medical Center, Cincinnati, Ohio; [4]Department of Pediatrics, University of Cincinnati College of Medicine, Cincinnati, Ohio; [5]Department of Physiology, Perelman School of Medicine, University of Pennsylvania, Philadelphia, Pennsylvania; [6]Department of Pathology, Children's Hospital of Philadelphia, Philadelphia, Pennsylvania; and [7]Department of Surgery, Perelman School of Medicine, University of Pennsylvania, Philadelphia, Pennsylvania

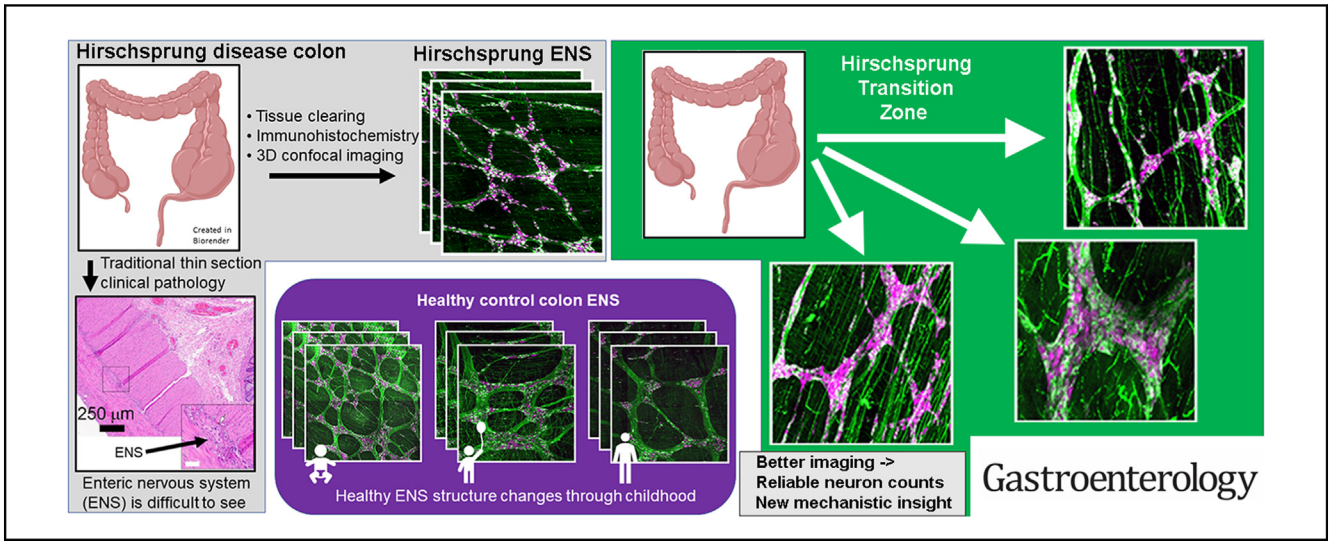

BACKGROUND & AIMS: Hirschsprung's disease is defined by the absence of the enteric nervous system (ENS) from the distal bowel. Primary treatment is "pull-through" surgery to remove bowel that lacks ENS, with reanastomosis of "normal" bowel near the anal verge. Problems after pull-through are common, and some may be due to retained hypoganglionic bowel (ie, low ENS density). Testing this hypothesis has been difficult because counting enteric neurons in tissue sections is unreliable, even for experts. Tissue clearing and 3-dimensional imaging provide better data about ENS structure than sectioning. **METHODS:** Regions from 11 human colons and 1 ileal specimen resected during Hirschsprung's disease pull-through surgery were cleared, stained with antibodies to visualize the ENS, and imaged by confocal microscopy. Control distal colon from people with no known bowel problems were similarly cleared, stained, and imaged. **RESULTS:** Quantitative analyses of human colon, ranging from 3 days to 60 years old, suggest age-dependent changes in the myenteric plexus area, ENS ganglion area, percentage of myenteric plexus occupied by ganglia, neurons/mm^2, and neuron Feret's diameter. Neuron counting using 3-dimensional images was highly reproducible. High ENS density in neonatal colon allowed reliable neuron counts using 500-μm^2 $\times$ 500-μm^2 regions (36-fold smaller than in adults). Hirschsprung's samples varied 8-fold in proximal margin enteric neuron density and had diverse ENS architecture in resected bowel. **CONCLUSIONS:** Tissue clearing and 3-dimensional imaging provide more reliable information about ENS structure than tissue sections. ENS structure changes during childhood. Three-dimensional ENS anatomy may provide new insight into human bowel motility disorders, including Hirschsprung's disease.

Keywords: Hirschsprung's Disease; Enteric Nervous System; Tissue Clearing; 3-Dimensional Imaging.

Hirschsprung's disease (HSCR) is a birth defect characterized by absence of the enteric nervous system (ENS) from the distal bowel. Because the ENS controls most aspects of bowel function, even short segments of "aganglionic" bowel (that lacks ENS ganglia) can cause intractable constipation, bilious vomiting, and predisposition to life-threatening sepsis. HSCR is treated via "pull-through surgery," a technique first developed in the 1940s.[1] In pull-through surgery, distal aganglionic bowel is removed and proximal ENS-containing bowel is reconnected near the anal verge. Despite this ostensibly curative surgery, HSCR-associated enterocolitis and functional obstructive symptoms are common before and after pull-through surgery.[2,3]

Why some children have problems after pull-though surgery, whereas others are free of symptoms, is not well understood. A common hypothesis is that postoperative HSCR-associated enterocolitis and obstructive complications occur because of incomplete removal of the transition zone, a region of decreased ENS density between normal and aganglionic bowel. Testing this hypothesis has been challenging because transition zone features are not easily defined using standard histology.

In the ENS, enteric neurons cluster into ganglia in 2 layers. Myenteric plexus ganglia between circular and longitudinal muscle control muscle contraction and relaxation. Submucosal plexus ganglia between circular muscle and bowel epithelium regulate epithelial function, blood flow, and immune cell activity in response to local stimuli. These interconnected neurons and associated glia are normally found along the entire bowel, but in children with HSCR, ENS is absent from distal bowel.

One important problem for HSCR clinical pathology is reliance on thin (4–15 μm) tissue sections. In thin sections, enteric neurons cannot be reliably counted, even by experts using immunohistochemistry to highlight neurons.[4] Furthermore, tissue sectioning makes it very difficult to identify 3-dimensional relationships between ENS cells clustered into small enteric ganglia of the myenteric and submucosal plexus. The low abundance (~1:10,000 colon cells are ENS) and irregular spacing of ENS cells means many tissue sections need to be evaluated to adequately sample ENS anatomy.[5] Reconstruction of serial sections would also be needed to visualize organization of the ENS, because many ENS defects can only be appreciated when the whole plexus is visualized, at least based on murine disease models.

Here we tested the hypotheses that tissue clearing, antibody staining, and 3-dimensional imaging could provide additional insight into HSCR mechanisms. We specifically hypothesized that ENS anatomy in small children might differ from ENS anatomy in adults and that ENS in children with HSCR might be very abnormal near the proximal edges of resected tissue, at least in some children. We also hypothesized that our 3-dimensional imaging method could facilitate more accurate quantitative analysis of human ENS anatomy than traditional sectioning.

WHAT YOU NEED TO KNOW

BACKGROUND AND CONTEXT

Clinical pathology relies on thin tissue sections that provide inadequate and unreliable information about enteric nervous system anatomy. Tissue clearing, immunohistochemistry, and 3-dimensional confocal imaging provide much better data.

NEW FINDINGS

Enteric nervous system anatomy changes throughout childhood. Three-dimensional imaging facilitates visualization of anatomy and identification of neurons, which could be valuable for bowel motility disorders, including Hirschsprung's disease.

LIMITATIONS

Additional study is needed to define anatomic features that correlate with good or bad postsurgical outcomes in Hirschsprung's disease. This technique requires 3 weeks and cannot be used intraoperatively.

CLINICAL RESEARCH RELEVANCE

The enteric nervous system controls most aspects of bowel function. Enteric nervous system defects cause Hirschsprung's disease, chronic intestinal pseudo-obstruction, and other bowel motility disorders. Many features of enteric nervous system anatomy cannot be seen in thin tissue sections but are easily appreciated via a simple clearing, staining, and 3-dimensional imaging strategy that is ideal for clinical research.

BASIC RESEARCH RELEVANCE

For most bowel motility disorders, anatomy of cells that control motility remains poorly defined because these cells are buried in an opaque bowel wall. By making the bowel translucent, staining structures of interest, and confocal imaging, diverse enteric nervous system features are readily visualized. These features help define disease mechanisms, a necessary step for development of mechanism-based therapy.

To test these hypotheses, we took advantage of a method we recently developed to analyze human ENS anatomy without tissue sectioning.[5] We examined colons resected from children with HSCR as part of standard care and compared ENS anatomy of HSCR colons against pediatric organ donor and adult colons. We discovered that human colon ENS anatomy changes between infancy and adulthood, even in people without known ENS disease. For HSCR colon, we found remarkably varied ENS features in the transition zone that would be difficult or impossible to appreciate in tissue sections.

Abbreviations used in this paper: **BABB, benzyl alcohol-benzyl benzoate; ChAT, choline acetyltransferase; ENS, enteric nervous system; HSCR, Hirschsprung's disease; HuC/D, human HuC/HuD neuronal protein; MEN2A, multiple endocrine neoplasia 2A; nNOS, neuronal nitric oxide synthase; PBS, phosphate-buffered saline; UW, University of Wisconsin.**

Most current article

© 2024 The Author(s). Published by Elsevier Inc. on behalf of the AGA Institute. This is an open access article under the CC BY-NC-ND license (http://creativecommons.org/licenses/by-nc-nd/4.0/).

0016-5085
https://doi.org/10.1053/j.gastro.2024.02.045

Materials and Methods

Human Tissue Acquisition

Colons were acquired with approval from the Children's Hospital of Philadelphia Institutional Review Board (IRB 13-010357) and the Perelman School of Medicine at University of Pennsylvania Institutional Review Board (IRB 804376). Human HSCR colons were obtained (1) with informed consent and full access to medical records or (2) deidentified with limited data (age, sex, and type of surgery). HSCR specimens were all obtained during clinically indicated pull-through surgery, using tissue not required for clinical pathology. We did not ask surgeons to resect tissue beyond what was clinically indicated. We focused on HSCR colon from primary pull-through procedures where aganglionosis was restricted to the colon, but examined the ileum from 1 child with total colonic aganglionosis. Pediatric organ donor colons were obtained from the Gift of Life Donor Program (Institutional Review Boards exempt). Pediatric specimens were compared with previously acquired data from adult colons.[5]

Tissue Processing

HSCR specimens were transferred from the operating room to Children's Hospital of Philadelphia pathology at room temperature. Bowel lumen was opened longitudinally along the antimesenteric border. Three segments were excised for clinical pathology, including proximal margin, distal margin, and a longitudinal strip all the way along the bowel (Figure 1*A*). Remaining tissue not required for clinical analysis was divided into the proximal neomargin (width approximately two-thirds of bowel circumference) and a longitudinal strip (width approximately one-third of bowel circumference).

Within 1 hour of tissue initial arrival in clinical pathology, these separate sections were placed into sterile ice-cold 1x phosphate-buffered saline (PBS) or in University of Wisconsin (UW) Belzer solution (NC0410019; Fisher Scientific, Waltham, MA). We received coded specimens in solution on ice. Colons from organ donors were placed immediately into UW Belzer solution on ice and transported to our laboratory. Organ donor colon lumen was opened longitudinally along the mesentery and cleared of stool. Descending colons from organ donors were evaluated to compare with HSCR pull-through segments because aganglionosis is restricted to the rectosigmoid colon in 80% of people with HSCR. For most imaging, taenia were avoided when they could be identified because thick taenia are more challenging to clear and image.

Human Colon Immunostaining and Clearing

Our detailed clearing and staining protocol was previously published, including step-by-step methods with details about reagents and sample handling.[5,6] Briefly, while specimens were in UW Belzer or PBS solution, visceral fat was removed, and tissue was stretched and pinned with serosa facing upward onto SYLGARD 184 Silicone Elastomer (Dow, Midland, MI), using insect pins (Figure 1*B*). Tissue was fixed overnight in 4% paraformaldehyde at 4°C. Then pins were removed. Tissue not immediately processed was stored in 50% glycerol, 50% PBS with 0.05% sodium azide at 4°C. Scissors were used to cut segments of fixed colon (Figure 1*C*). Stained regions were usually ~5 mm × 5 mm. Segments were initially washed in PBS (3 × 5 minutes at room temperature), permeabilized with 100% methanol (1 hour on ice), treated with Dent's bleach (2 hours at room temperature), and placed in blocking solution (3 days on a shaker at 37°C).

This was followed by incubation in primary antibody (Supplementary Table 1) (14 days at 37°C) on a shaker. Tissue was then washed in PBS (2 × 2–3 hours, and 1× overnight), followed by incubation in secondary antibody (Supplementary Table 1) (3 days at 37°C) on a shaker, dehydrated in serial methanol dilutions, and cleared with benzyl alcohol-benzyl benzoate (BABB) (1:2) until tissue was translucent (Figure 1*D*). Tissue was mounted on glass slides in BABB for imaging (Figure 1*E*).

For the 3-day-old organ donor, we imaged full-bowel circumference. For the 5-year-old organ donor, we imaged half the colon circumference. To image these large areas, we devised a new mounting method that flattens tissue more completely (Supplementary Figure 1) and used ethyl cinnamate as the mounting medium instead of BABB, which preserved tissue for imaging for months.

Image Acquisition and Analysis

Most cleared tissue was imaged on a Zeiss LSM 710 confocal microscope (10×/0.3 and 20×/0.8 Plan-Apochromat objectives, and Zen 2.3 14.0.14.201 software (Zeiss, Oberkochen, Germany). *Z*-axis intervals were 4 μm (10× objective) or 1 μm (20× objective). For each segment imaged, confocal Z-stacks were obtained with 10× objective using tile scan (5% overlap) and stitch features to visualize large regions of full-thickness tissue. Multichannel images were acquired sequentially using laser-scanning operated under multitrack. Excitation/long-pass emission filters were Alexa Fluor 488, Alexa Fluor 594, and Alexa Fluor 647. Full- and half-circumference imaging from organ donor colons was obtained on a Zeiss LSM 980 confocal microscope (Plan-Apochromat 10×/0.45 working distance = 2.0 M27, Zeiss Zen Blue 3.5 software, variable laser power) at 2-μm intervals (5% overlap).

Full-thickness Z-stacks were used for myenteric plexus area and submucosal plexus assessments. Four additional images per segment (708 μm^2 × 708 μm^2) were obtained with a 20× objective, 1 in each quadrant. These Z-stacks were used for neuron density and subtype counting. Image analysis was performed using ImageJ (Java 1.8), including features of Z-project, scale bar, polygon selection, rectangle selection, specify, straight line tool, measurements, cell counter, and regions of interest manager.

Quantitative Analysis of Myenteric Plexus Density

Two-dimensional flattened Z-stacks obtained with a 10× objective were manually outlined. The myenteric plexus was defined as myenteric ganglia and thick neuron fiber bundles between ganglia. Areas selected for analysis were the largest contiguous rectangular areas in which plexus was visible in the plane of flattened Z-stacks. Ganglia were defined as clusters of >1 neuron soma separated by <1 soma diameter. Individual ganglia were separately outlined. We calculated the percentage of bowel wall containing plexus, the percentage of bowel wall containing ganglia, and the percentage of the plexus containing ganglia.

Quantitative Analysis Neuron Subtypes and Size

Myenteric plexus neurons (HuC/D+) were counted manually in 3-dimensional 20× Z-stacks. For each bowel region, we counted all neurons in randomly selected 500-μm × 500-μm regions (1 region in each quadrant of stained tissue). Data are

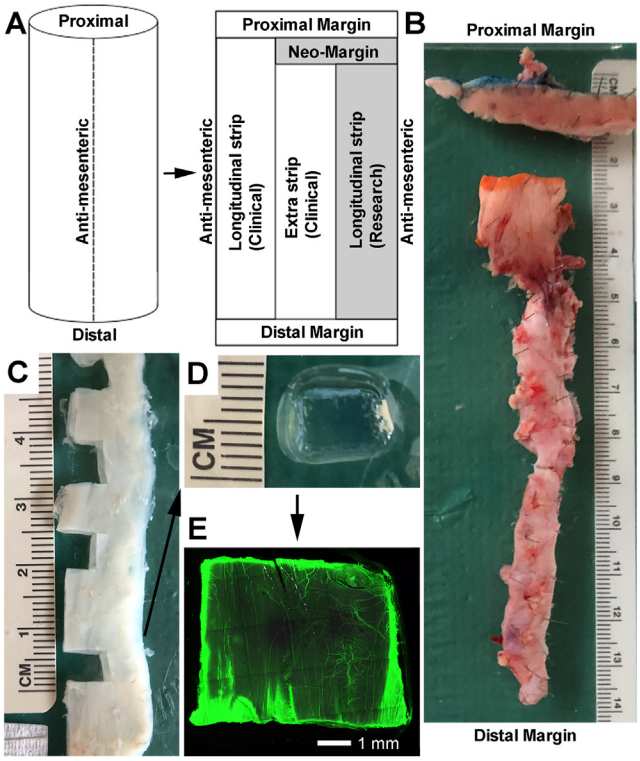

Figure 1. Colon analysis strategy. (*A*) Schematic of HSCR pull-through tissue obtained from clinical pathology. (*B*) Neomargin and longitudinal strip of bowel from HSCR colon resection stretched and pinned on a SYLGARD-coated plate. (*C*) Fixed human colon with ~ 0.5-cm × 0.5-cm sections removed for staining and imaging. (*D*) Human colon resected from a child with HSCR after tissue clearing and staining with HuC/D (*magenta*) and nNOS (*green*) antibodies. (*E*) Tissue from panel *D* was imaged using confocal microscopy, demonstrating the near complete absence of ganglion cells in the entire imaged region.

presented in neurons per mm^2. Neurons expressing neuronal nitric oxide synthase (nNOS, NOS1) were counted as nitrergic. Neuron size was measured as the longest Feret's diameter.

Statistics

Analyses used Prism 7 (GraphPad Software, San Diego, CA) and RStudio Version 1.4.1717 (ggplot2, ggpubr, tidyverse, broom, and dplyr packages). D'Agostino-Pearson tests were used to assess normality. Unpaired *t* tests were used to compare means of normally distributed data. Paired *t* tests were used to compare means of repeated counts of the same images for interobserver variability. Mann-Whitney tests were used to compare means of nonnormally distributed data. Data are presented as mean ± standard error of the mean. Best fit lines are plotted as linear regression.

Results

We obtained tissue from 16 children with HSCR undergoing primary (ie, first) pull-through surgery, and from 3 human organ donors (Supplementary Table 2). The organ donors were 3 days, 5 years, and 18 years old and had no known bowel disease. Of the 16 HSCR pull-through children, 2 have total colonic aganglionosis (HSCR12, HSCR16), 1 has Down syndrome (trisomy 21) (HSCR13), 1 has multiple endocrine neoplasia 2A (MEN2A) (*RET* (c.1858T>G, p.Cys620Gly in exon 10) (HSCR11), and 1 has cystic fibrosis (HSCR8). Two were not evaluated because additional colon was resected during the primary surgery but was not available to our laboratory (HSCR14, HSCR15). Colon from the child with Down syndrome had no neurons in the proximal resection neomargin, so quantitative analyses were not pursued. Terminal ileum from HSCR12 was imaged and compared with control ileum from 1 organ donor. For the 12 HSCR pull-through segments imaged and analyzed, there were 4 different surgeons.

These data highlight the complexity of HSCR and HSCR surgery. To interpret data from HSCR resections, we evaluated ENS anatomy in the distal colon from the pediatric organ donors presumed to have normal ENS anatomy (control 1, control 2, and control 3) and in adult descending colons (adult 1–adult 4) previously analyzed by our group.[5]

Imaging Enteric Nervous System Anatomy in Human Colon Without Tissue Sectioning

To visualize interconnections between enteric ganglia of myenteric and submucosal plexus, we pursued 3-dimensional confocal imaging in cleared human colon without sectioning. Our surgeons performed their usual pull-through surgery. Our clinical pathologists took tissue needed for clinical care and provided us with remaining bowel that would normally be discarded (Figure 1*A*). For organ donors we analyzed descending colon, the most common region for proximal resection margin in HSCR pull-through surgery. Tissue was pinned flat and fixed (Figure 1*B*). Then, 5-mm × 5-mm pieces were cut with a scissors (Figure 1*C*), stained with antibodies, and cleared (Figure 1*D*) to make the colon translucent before confocal imaging (Figure 1*E*).

Antibodies to HuC/D and neuronal nitric oxide synthase (nNOS, NOS1) reliably stained human colon with our method. HuC/D antibody stains ELAV family proteins in the cell body marking all enteric neurons. nNOS antibody stains nerve cell bodies and neuronal fibers for inhibitory motor neurons and descending interneurons in myenteric plexus.[7]

The 416 confocal Z-stacks we generated are available as supplementary data (Supplementary Table 3). Selected Z-stacks were converted to videos to show images analyzed (Supplementary Videos 1-31b, 55 total; Supplementary Table 3). All videos and images will be available via the SPARC Data Portal (https://sparc.science/). Staining tissue in this manner allowed for visualization of both overall ENS structure and two neuron classes: nitrergic neurons (nNOS-positive) and nonnitrergic neurons (nNOS-negative).

Characterization of Pediatric Myenteric Plexus in Organ Donor Colon

Because most people with HSCR have pull-through surgery as infants or toddlers, interpreting HSCR ENS anatomy requires data about normal human colon ENS at various ages. On the basis of murine data, we hypothesized that the

quantitative features of ENS anatomy we described in adult colon might differ from pediatric ENS.[5,8] To test this hypothesis, we first compared HuC/D and nNOS antibody-stained myenteric plexus from 3-day-old organ donor colon (Figure 2*A*) with adult colon myenteric plexus (Figure 2*D*). The 3-day-old colon ENS appeared far denser and comprised a larger percentage of bowel wall area than adult colon ENS.

To pursue this observation, we determined the percentage of bowel wall occupied by myenteric plexus (Figure 2*E* and *F*), the percentage of bowel wall occupied by myenteric ganglia (Figure 2*G* and *H*), and the proportion of

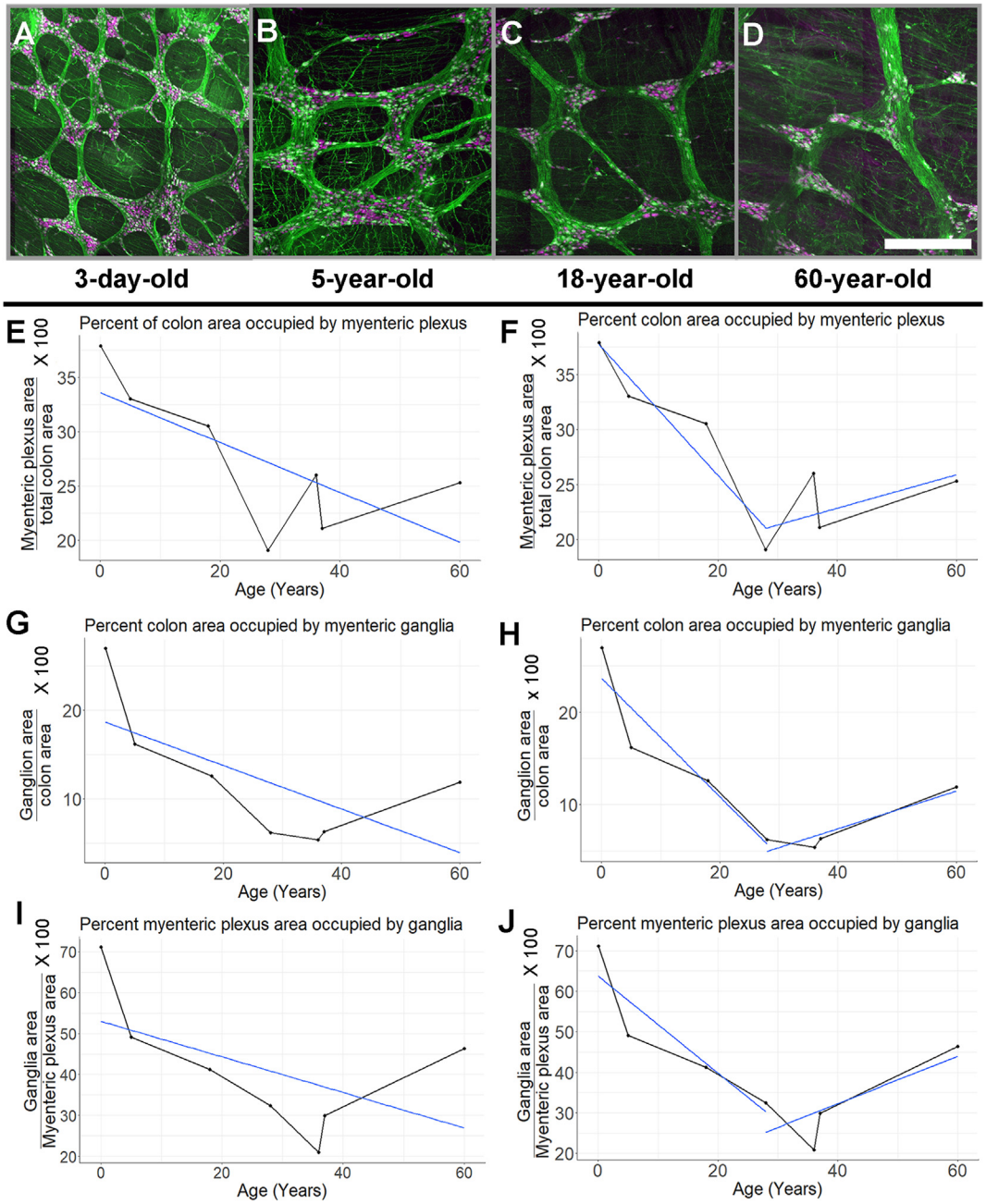

Figure 2. Normal colon myenteric plexus anatomy varies with age. (*A–D*) Flattened Z-stacks of myenteric plexus stained with antibodies to HuC/D (*magenta*) and nNOS (*green*). Descending colon from (*A*) 3-day-old, (*B*) 5-year-old, and (*C*) 18-year-old organ donors with no known bowel dysfunction. (*D*) Descending colon from a 60-year-old individual adjacent to resected diverticulitis. Tissue sections looked normal by H&E staining. *Scale bar* = 500 μm. (*E–J*) Quantitative analyses of myenteric plexus using maximum intensity Z-projections. Percentage of flattened Z-stack containing (*E* and *F*) myenteric plexus (ganglia plus thick nerve fiber bundles) and (*G* and *H*) myenteric ganglia (clusters of nerve cell bodies). (*I* and *J*) Percentage of myenteric plexus within the Z-stack occupied by myenteric ganglia. (*E*, *G*, and *I*) Linear regression shows a single *best fit line* based on all data. (*F*, *H*, and *J*) Same data as in panels *E*, *G*, and *I* showing separate linear regressions for 3-day-old to 28-year-old and for 28-year-old to 60-year-old data sets.

myenteric plexus occupied by ganglia (Figure 2*I* and *J*) within the myenteric plexus plane (Supplementary Table 4). Similar analyses were pursued using 5-year-old and 18-year-old organ donor distal colon (Figure 2*B* and *C*) and using distal colon from 28-, 36-, 37-, and 60-year-old adults with no history of bowel dysfunction.

These data show the proportion of bowel wall occupied by myenteric plexus and by myenteric ganglia progressively declined from birth to age 28 years, as did proportions of myenteric plexus occupied by ganglia (Figure 2*E*–*J* and Supplementary Table 4). We initially tried fitting data from 3-day-old to 60-year-old colons to a single linear regression (Figure 2*E*, *G*, and *I*) but discovered the data fit better to separate pediatric and adult linear regressions (Figure 2*F*, *H*, and *J*). Collectively these data confirm the need for age-specific quantitative data about ENS anatomy and suggest that myenteric plexus and ganglion cell density declines as children grow and the colon enlarges.

Minimal Interobserver Variability for Neuron Counting in Z-Stack Images

Neuron counting is notoriously difficult for human ENS, leading to discrepancies even between expertly trained pathologists.[4,9] We hypothesized that neurons in 3-dimensional confocal images could be more reliably counted than neurons in tissue sections currently used by pathologists (Figure 3). To test this hypothesis, a new investigator counted neurons in 15 adult colon confocal 20× Z-stacks our group previously analyzed.[5] These images were stained for HuC/D, nNOS, and choline acetyltransferase (ChAT), permitting us to define 4 neuron subtype classes. Counts were performed blinded so the new investigator was unaware of prior results. When data from 15 regions were combined, there were no statistically significant differences between any neuron subtype counts for the 2 observers (Figure 3*A*). For individual regions, neuron counts agreed closely for all HuC/D+ neurons ($R^2 = 0.94$), total nNOS+ neurons ($R^2 = 0.84$), and total ChAT+ neurons ($R^2 = 0.74$) (Figure 3*B*), but varied more for scoring "Neither nNOS nor ChAT" ($R^2 = 0.61$), probably because ChAT staining is not ideal as we previously reported (Supplementary Table 5).[5] These observations suggest that 3-dimensional imaging facilitates reliable neuron counting when staining is effective.

Neuron Count Reliability as a Function of Area Using Z-Stack Images

Because enteric neurons cluster into ganglia, neuron counts depend on which region is counted and how large a region is analyzed. To assess the minimum bowel area required for reliable neuron counts in a 3-day-old infant, a representative 700-μm × 700-μm (20×) image was divided into 49 squares (each square = 100 μm × 100 μm) (Figure 3*C*). Neurons were manually counted in each square, revealing convergence of neuron counts/mm^2 when areas analyzed measured 5 squares × 5 squares (Figure 3*D*). To ensure reliability in our data, we therefore counted neurons in 500-μm × 500-μm areas in pediatric colons for subsequent analyses.

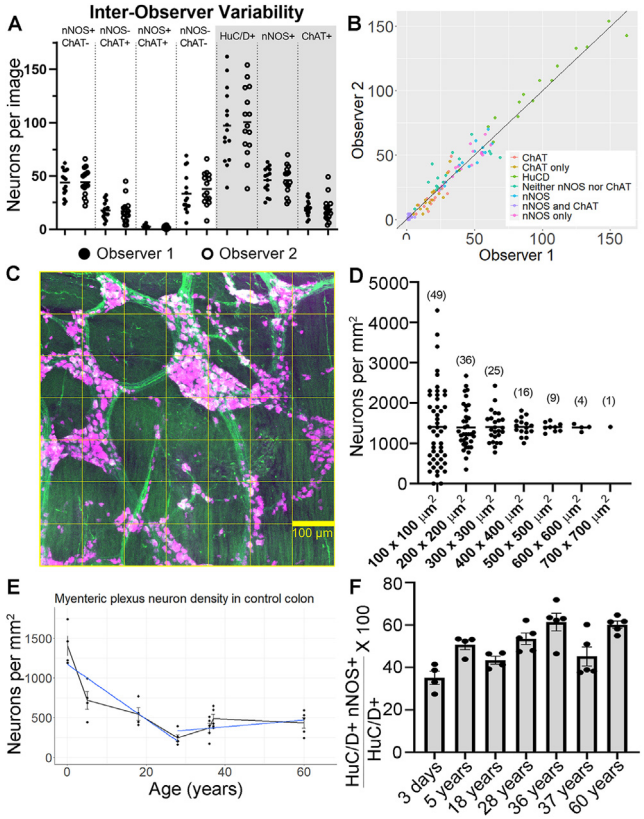

Figure 3. Three-dimensional confocal Z-stacks provide reliable estimates of neuron density and percentage of nNOS-expressing neurons in human colon. (*A*) Comparison of myenteric plexus cell counts by 2 independent observers using the exact same colon 3-dimensional confocal Z-stacks. Neuron subtypes were identified by staining with HuC/D, nNOS, and ChAT antibodies. *Circles* show neuron counts from each of 15 images (3 adults, 5 images each, dimensions 708 μm × 708 μm × 40–123 μm). All subtype counts by each observer were normally distributed. All interobserver differences were statistically equivalent by paired *t* test. *Lines* indicate mean neuron counts. (*B*) Plot shows neuron counts for 15 individual images evaluated by 2 observers. The R^2 values varied among neuronal subtypes and are reported in the text. (*C*) Flattened 126-μm thick Z-stack of myenteric plexus from colon of 3-day-old human organ donor divided into 49 squares (100 μm × 100 μm each). (*D*) Each *circle* shows counts obtained from a region of the size indicated on the *x*-axis from the Z-stack depicted in image *C*. The *horizontal lines* indicate mean values. (*E*) Quantitative analysis of myenteric plexus neuron density using Z-stacks obtained with a 20× objective. All neurons were counted in 4 to 5 regions (500 μm × 500 μm each) per individual. Linear regression shows *best fit lines* for 3-day-old to 28-year-old and for 28-year-old to 60-year-old colon. (*F*) Percentage of myenteric neurons that are nitrergic (HuC/D+ nNOS+) at various ages. The *error bars* indicate the standard error of the mean.

Neuron Density, Percentage of Nitrergic Neurons, and Neuron Size Differ in Infants and Adults

Analyzing regions between taenia, we found that myenteric plexus neuron density in control colons declined during childhood (Figure 3*E* and Supplementary Table 6), whereas the percentage of myenteric neurons that were

nNOS+ increased (Figure 3*F* and Supplementary Table 6). Myenteric neurons in the 3-day-old control colon were smaller than in older colons (Supplementary Figure 2*A*) based on the longest neuron Feret's diameter (3-day-old = 13.0 ± 0.46 μm, 5-year-old = 20.7 ± 0.92 μm, and 18-year-old = 22.8 ± 0.99 μm; $P < .0001$ vs 3-day-old for both older ages). There was no statistically significant difference in neuron Feret's diameter between 5-year-old and 18-year-old colons ($P = .115$). Additionally, there was no difference in neuron size between nitrergic and nonnitrergic neurons in control pediatric colons assessed (Supplementary Figure 2*B*).

Enteric Neuron Density Is Similar in Regions With and Without Taenia

To evaluate how ENS structure varied around the bowel circumference, we imaged the entire bowel width in the 3-day-old organ donor after HuC/D and nNOS antibody staining (Figure 4 and Supplementary Figure 3). Enteric neuron density varied little across the bowel circumference, including in regions with and without taenia (neurons/mm^2: taenia, 1889.0 ± 22.2; nontaenia, 1962.0 ± 78.9; $P = .34$). In the 5-year-old organ donor, we could only visualize half the bowel circumference before files became too large for imaging software to open. ENS density also appeared similar around the 5-year-old colon circumference, and neuron counts were similar in regions with and without taenia (neurons/mm^2: taenia, 806.0 ± 29.41; nontaenia, 770 ± 35.34; $P = .69$ by Mann-Whitney *U* test). Because thick muscle bands in taenia make imaging more challenging, all other images were from regions between taenia.

Myenteric Plexus in Hirschsprung's Disease Proximal Resection Margin Varied Markedly Among Children

One primary goal of evaluating ENS anatomy in control distal colon (Figures 2 and 3, Supplementary Figures 2 and 4, Supplementary Videos 29–31 and 52–55, Supplementary Table 3 confocal Z-stacks 231-284 and 413-416, and Supplementary Tables 3–6) was to put in context ENS anatomy in children with known or suspected ENS disease, including HSCR. For HSCR, surgeons remove distal bowel that lacks ENS and attempt to remove the hypoganglionic "transition zone" that is presumed dysfunctional. The decision about how much bowel to remove is made in the operating room based on frozen sections (15 μm) from small biopsy specimens, but these sections provide limited views of ENS anatomy (Figure 5*A*, Figure 6*Y* and *Z*, Figure 7*U* and *V*, and Supplementary Figure 5*I*).

To gain deeper insight into HSCR anatomy, colon 0.5 cm to 2.4 cm from the proximal pull-through resection margins was cleared, stained with antibodies (HuC/D, nNOS), and imaged by confocal microscopy. Full-thickness regions ∼5 mm × 5 mm were imaged. Confocal images demonstrated striking variability in HSCR proximal margin ENS anatomy (Figure 5*B–K*). Myenteric plexus area in proximal margins varied from 16.0% to 59.7% of the total colon area, whereas ganglia occupied 14.7% to 70.4% of the myenteric plexus (Supplementary Table 4). The mean density of myenteric plexus neurons varied >8-fold (range, 234–1972 neurons/mm^2), with no apparent correlation to age at the time of surgery (Figure 5*B–L* and Supplementary Table 6). The percentage of nitrergic neurons at the proximal margins of children with HSCR also varied considerably (range, 28%–63%) but these percentages were similar to values in organ donor colons (Supplementary Figure 4 and Supplementary Table 6).

Complex Features of Hirschsprung's Disease Transition Zone Enteric Nervous System Anatomy

To characterize the transition zones of HSCR colon (HSCR1 to HSCR11), we stained tissue from proximal resection margins plus 1 to 2 additional distal regions with antibodies to HuC/D and nNOS (Figures 6 and 7 and Supplementary Figures 5–8). Assessed transition zones had thin nerve fiber bundles between ganglia in the myenteric and submucosal plexus in addition to the gradual disappearance of neurons distally. In some children, the transition zone appeared to terminate at the same distance from the proximal margin in both myenteric and submucosal plexus (Figure 6*E–H*, Figure 7*I–L*, and Supplementary Figure 6*A–H*). In other children, the transition zone extended over a longer distance in the myenteric plexus compared with the submucosal plexus (Supplementary Figure 8*E–L*), and in some cases, the opposite was true (Supplementary Figure 8*U–X*). In one child, a cluster of HuC/D+ cells organized atypically was present in muscularis propria within a region of aganglionosis (Supplementary Figure 6*Q–T*).

Analysis of neuron density at various distances from proximal margins demonstrated different degrees of hypoganglionosis throughout the transition zone. The transition zone-aganglionosis border ranged from 3.2 cm to >13 cm distal to the proximal resection margin (Figure 5*L*). These features of the transition zone would be very challenging to appreciate using any standard clinical pathology technique. The difficulty assessing ENS anatomy is further emphasized by our analysis of HSCR11, a 5.3-month-old with MEN2A (Supplementary Figure 5). Although we found 1451 neurons/mm^2 at the proximal resection margin of the colon we received (similar to 3-day-old organ donor control), intraoperative assessment of ENS anatomy led to a decision to remove an additional 23.5 cm of more proximal colon (not available to us). Finally, we imaged distal ileum from a child with total colonic aganglionosis (HSCR12). Compared with ileum from the 5-year-old organ donor (control 2), ENS appeared sparse in the HSCR ileum (Supplementary Figure 9).

Discussion

Anatomic defects underlying bowel motility disorders remain incompletely understood, in part because human ENS is difficult to visualize through the opaque colon wall. Although most prior ENS studies use tissue sectioning, this approach provides very limited views of ENS anatomy and

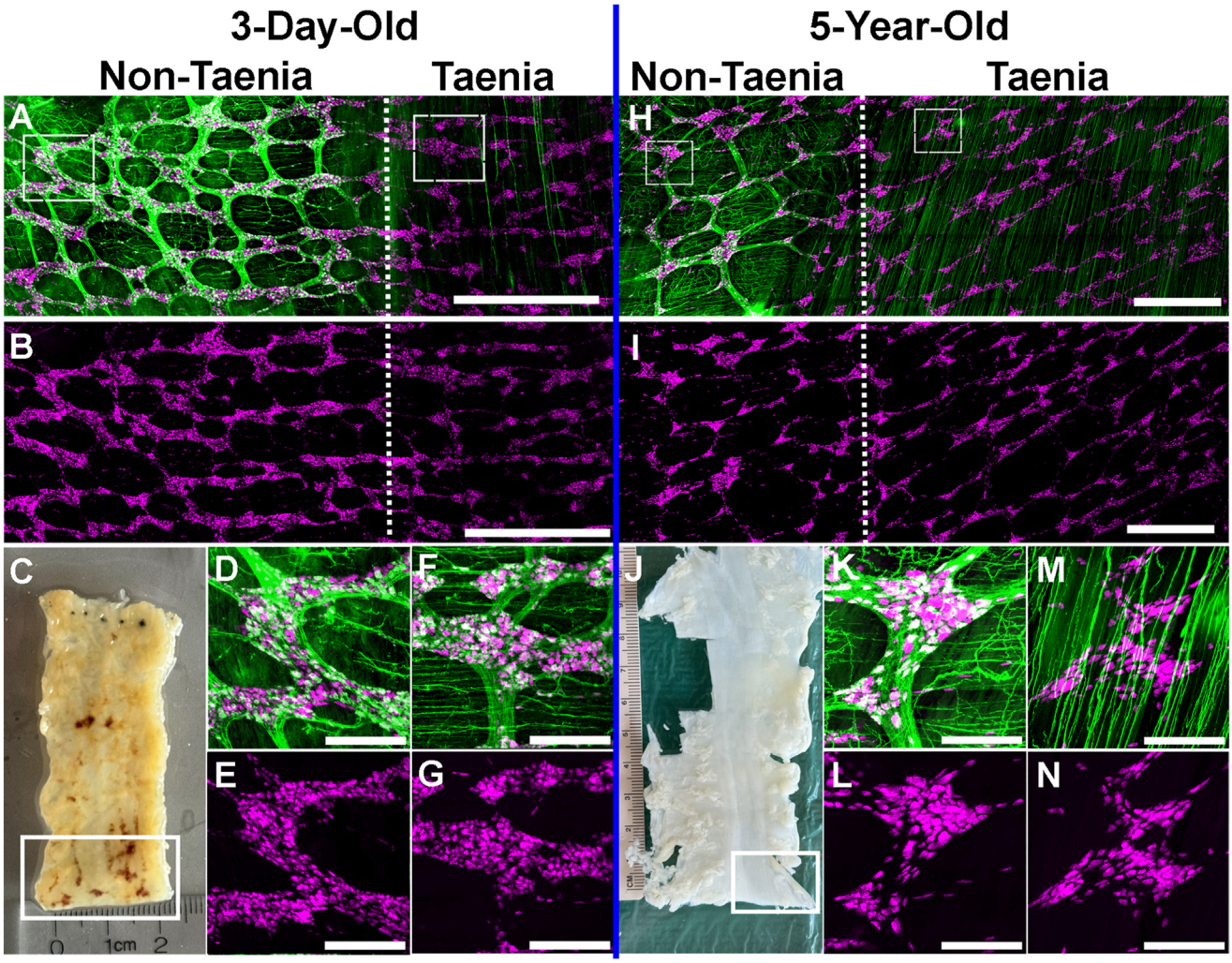

Figure 4. Myenteric neuron density is similar in regions with taenia and between taenia. Full-thickness descending colon from organ donors stained with HuC/D (*magenta*) and nNOS (*green*) antibodies imaged at 10× (2-μm intervals between confocal slices). Images from (*A–G*) 3-day-old and (*H–N*) 5-year-old colons were selected from larger full-circumference or half circumference (respectively) Z-stacks in Supplementary Figure 3*C–F*. (*A*, *B*, *D–G*, *H*, *I*, and *K–N*). Flattened Z-stacks from the myenteric plexus region. (*A*, *B*, *H*, and *I*) The *dotted lines* separate regions with or without taenia. (*C* and *J*) Gross tissue indicating regions imaged. (*B*) HuC/D of region in panel *A*. (*I*) HuC/D of region in panel *H*. Enlarged images of regions in *boxes* at the (*D* and *E*) *left* or (*F* and *G*) *right* in panels *A* and *B*. Enlarged images of regions in *boxes* at the (*K* and *L*) *left* or (*M* and *N*) *right* in panels *H* and *I*. *Scale bar* = 1000 μm in *A* and *H*. *Scale bar* = 200 μm in *D–G* and *K–N*.

can be misleading because enteric neurons and glia cluster into ganglia. This clustering means that some sections in normal human colon have many enteric neurons and other adjacent sections have no neurons.[5] Furthermore, even for experts, it is challenging to unambiguously identify enteric neurons in tissue sections, as elegantly demonstrated by Swaminathan and Kapur.[4] These problems probably explain the 150-fold range for "normal" human colon enteric neuron density reported in the literature.[4]

To overcome these problems, a few prior studies have used tissue microdissection, which provides much better views of ENS anatomy.[10,11] However, microdissection requires specialized skills, disrupts normal structures, does not visualize submucosal neurons well, and is labor intensive. In contrast, we visualized ENS in human colon without sectioning using a recently developed and simple method for tissue clearing, immunohistochemistry, and confocal imaging. Our analyses demonstrate substantial changes in ENS anatomy during childhood, indicating the need for age-specific normal ranges. Our studies also show remarkable diversity of ENS structures in children with HSCR, an observation that might underlie variable outcomes after HSCR pull-through surgery.

Colon Enteric Nervous System Anatomy Changes as Children Grow

To determine whether ENS anatomy at the proximal resection margin predicts outcomes after HSCR surgery, we first need to define normal ENS anatomy. Our data show that "normal" varies depending on the age of the individual, confirming and extending prior results in rodents and

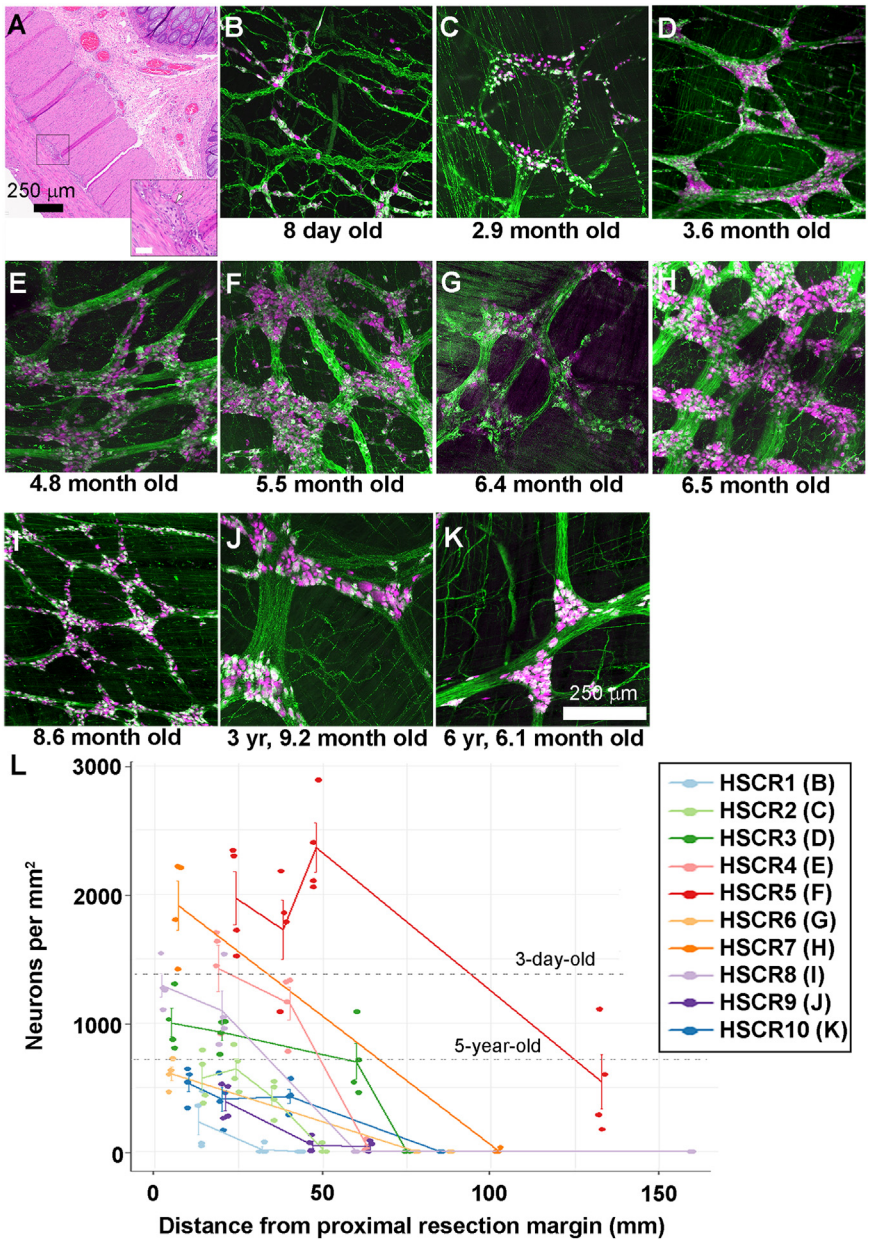

Figure 5. Colon myenteric plexus in HSCR disease varies considerably at the proximal surgical margin. (*A*) H&E-stained clinical pathology section of colon proximal margin from an HSCR pull-through surgery (HSCR1, 13 mm from proximal margin). *Scale bar* = 250 μm. ENS is difficult to see in these sections, even when the myenteric plexus region (*boxed*) is enlarged ~3.5-fold (*inset*, *scale bar* = 50 μm). The *arrow* points to a myenteric neuron. (*B–K*) Representative images (original magnification ×20) from colon myenteric plexus of HSCR1 to HSCR10 were stained with antibodies to HuC/D (*magenta*) and nNOS (*green*). The key in *panel L* indicates how each HSCR number matches *panels B–K*. Images show flattened 3-dimensional Z-stacks at the proximal neomargin of HSCR pull-through segments. *Scale bar* = 250 μm. (*L*) Neurons/mm^2 in Z-stacks containing myenteric plexus at varied distances from the proximal resection margin. The *dots* indicate mean neuron counts in four 500-μm^2 × 500-μm^2 regions per colon at each location. The *error bars* indicate the standard error of the mean. The *horizontal dashed lines* indicate mean neuron counts for the 3-day-old (control 1) and 5-year-old (control 2) colon ENS. The *key* indicates colors for the lines in *panel L* and correlation between HSCR numbers (HSCR1 to HSCR10) and *panels B–K*. "HSCR1 (*B*)" in the *key* indicates that the image in *panel B* was from HSCR1. The same logic applies to all HSCR numbers.

humans.[12–15] We focused on the distal colon because this region is most commonly resected from children with HSCR, recognizing that ENS anatomy varies between bowel regions.[16] Consistent with prior studies,[15] our images show neonatal human colon myenteric neurons in closely spaced ganglia. Between the ages of 3 days and 28 years, there was a progressive decline in the percentage of colon containing myenteric plexus, the percentage of myenteric plexus containing ganglia, and the density of myenteric neurons. Individual myenteric neurons were also smaller in young children than in adults.

These data provide a framework for understanding human distal colon ENS anatomy and make it obvious how inadequate sampling might provide misleading information. Because neonatal myenteric ganglia are closely spaced, our analyses suggest that reliable enteric neuron counts can be obtained from a 500-μm^2 × 500-μm^2 (250,000 μm^2) region in neonates. In contrast, our prior adult data suggested 3-mm^2 × 3-mm^2 regions were needed for reliable neuron counts (a 36-fold larger area).

Consistent with our data, Swaminathan and Kapur,[4] using tissue sections, showed that reliable data from 8-week-old human rectum required neuron counts in at least 5 full circumference regions. Because Swaminathan and Kapur evaluated 4-μm sections separated by at least 24 μm, we estimate that 5 full circumference regions covered 500,000 μm^2 (5 sections × 4-μm thick × 25,000 μm [circumference estimate] = 500,000 μm^2) or 3,500,000 μm^2 (5 sections × [4-μm thick + 24-μm spacing] × 25,000 μm [circumference estimate] = 3,500,000 μm^2), if including spacing between

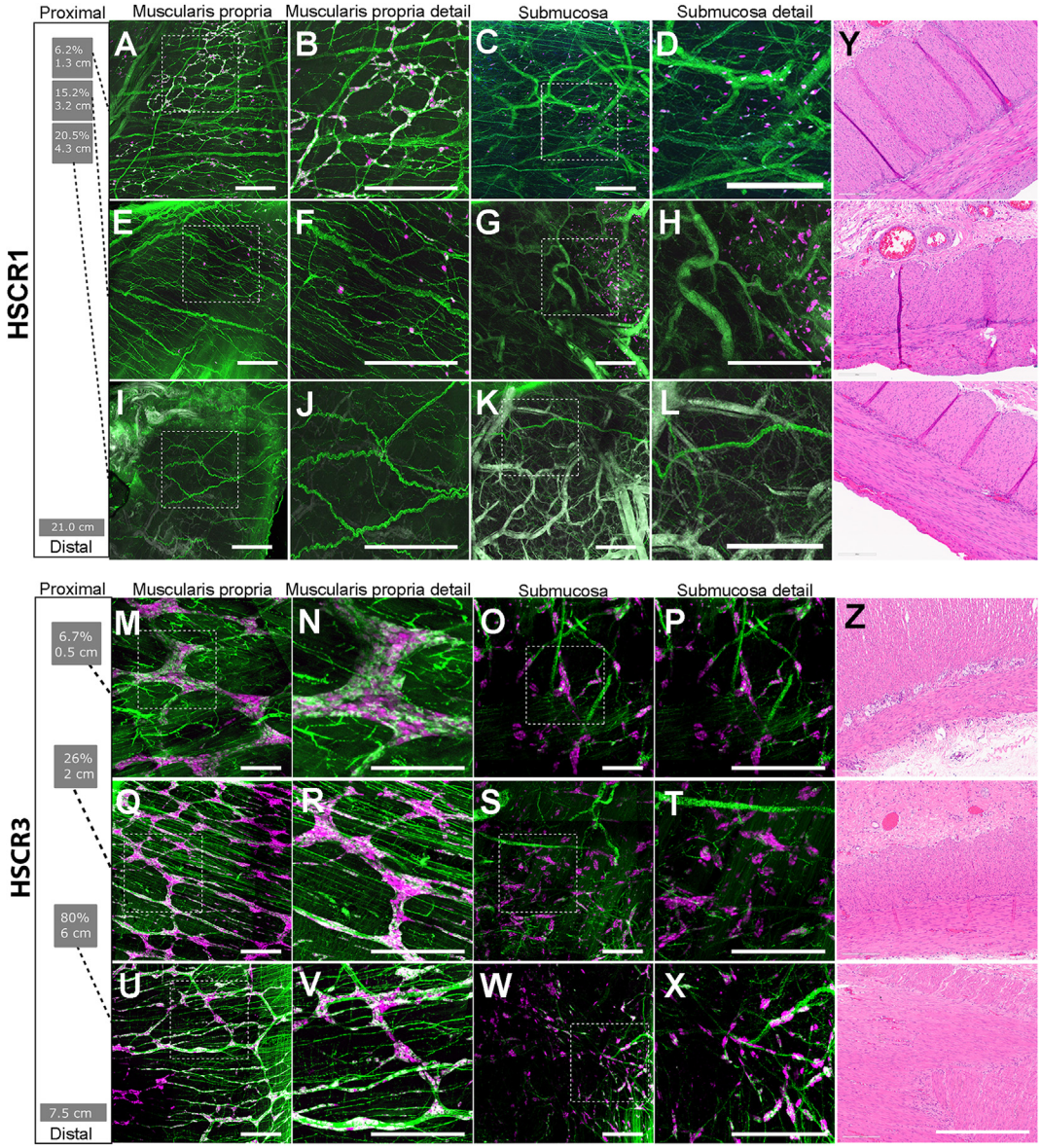

Figure 6. HSCR transition zone anatomy for HSCR1 and HSCR3. (*A–X*) Representative flattened Z-stacks show myenteric and submucosal plexus at various locations in resected colon stained with antibodies to HuC/D (*magenta*) and nNOS (*green*). The *second* and *fourth columns* show magnified views of *boxed areas* in the *first* and *third columns* respectively. Schematics to the *left* of images indicate distance in cm from the proximal resection margin and relative location (% = distance from proximal margin/length of resected bowel × 100). (*Y* and *Z*) H&E-stained colon sections (4 μm) from the same region as the 3-dimensional confocal images on the same *horizontal row*. *Scale bars* = 500 μm.

sections. Neither of these analyses considers the possibility that neuron density might vary around the bowel circumference, as suggested by Swaminathan and Kapur. However, our full-circumference or half-circumference images from 3-day-old and 5-year-old organ donor colons show ENS ganglia distributed all the way around the bowel wall, with similar enteric neuron density in regions with and without taenia.

Three-Dimensional Imaging Permits Highly Reproducible Quantitative Analysis

Another key observation from Swaminathan and Kapur[4] is that counting enteric neurons is difficult in thin tissue sections. Even with nicely stained immunohistochemically marked neurons, specific criteria for what should be counted, repeated training, and expert pathologists, their inter-observer counts varied by up to 5-fold for the exact same slides. In contrast, using our 3-dimensional confocal images, HuC/D-stained neuron counts varied on average by 7% (and at most by 20%) for the exact same image analyzed by 2 observers. This >25-fold improvement in the accuracy of neuron counts probably occurs because it is easier to unambiguously identify an enteric neuron in 3-dimensional Z-stacks than in thin sections. Our 3-dimensional neuron counts for nNOS+ enteric neurons also varied by an average of 8% between observers (and at most 18%) for any image.

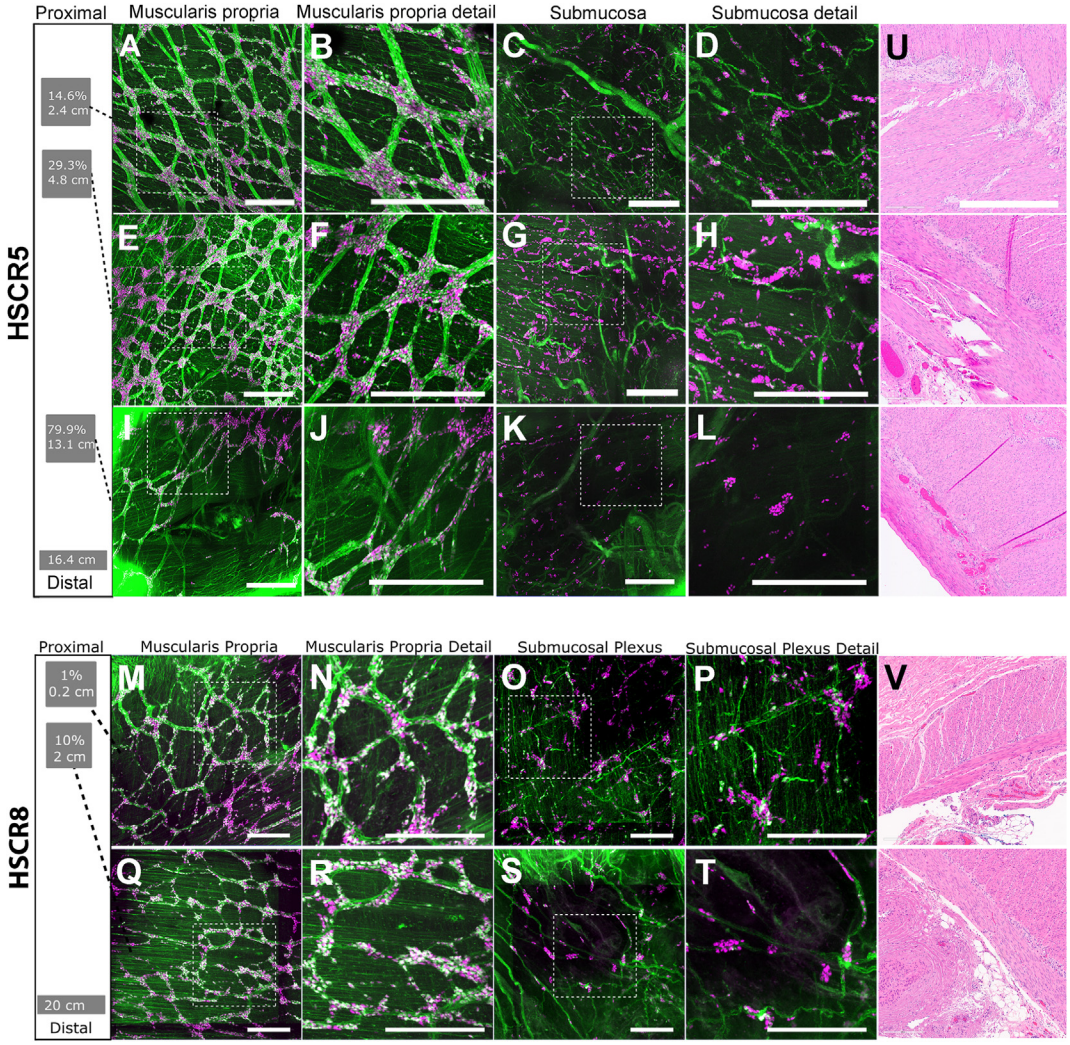

Figure 7. HSCR transition zone anatomy for HSCR5 and HSCR8. (*A–T*) Representative flattened Z-stacks show myenteric and submucosal plexus at various locations in resected colon stained with antibodies to HuC/D (*magenta*) and nNOS (*green*). The *second* and *fourth columns* show magnified views of *boxed areas* in *first* and *third columns*, respectively. Schematics to the *left* of images indicate distance in cm from the proximal resection margin and relative location (% = distance from proximal margin/length of resected bowel × 100). (*U* and *V*) H&E-stained colon sections (4 μm) from the same region as the 3-dimensional confocal images on the same *horizontal row*. *Scale bars* = 500 μm.

HuC/D and nNOS antibodies both stain tissue beautifully, but even for ChAT antibody, where staining is more challenging to interpret, average interobserver counts varied by only 28%. Thus, in addition to providing data about how the ENS is organized, neuron counting is dramatically better in confocal Z-stacks than in tissue sections.

New Insight Into Enteric Nervous System Anatomy in Hirschsprung's Disease

Children with HSCR undergo pull-through surgery where distal aganglionic bowel is removed and surgeons determine the proximal resection margin based on small biopsy specimens and frozen sections. In our studies, the ENS in colon just distal to the resection margin varied dramatically among children with HSCR. Some specimens had only a few small ganglia with very thin nerve fibers, whereas others had thick nerve fiber bundles connecting large dense ganglia. Quantitative analysis showed neuron density similar to pediatric organ donors in 6 of the 10 proximal margins evaluated (within ~30% of controls). The other 4 HSCR colons had 3.4-fold to 8-fold fewer neurons near the proximal resection margin compared with the most densely innervated colon resected.

Although low neuron density might be predicted to lead to poor postoperative outcomes, HSCR1 had the fewest enteric neurons/mm^2 near the proximal resection margin and did well after surgery. During 31 months follow-up, he was hospitalized only once (5 months after pull-through) because of vomiting and diarrhea. Although these are HSCR-associated enterocolitis symptoms, he had norovirus, respiratory syncytial virus, and rhinovirus at the time of admission, making infectious enteritis most likely. Other than this episode, HSCR1 ate well and grew well, without obstructive symptoms or enterocolitis after pull-through surgery. These observations suggest we have more to

learn about anatomic features that predict good or bad outcomes after HSCR surgery.

Three-dimensional ENS imaging also revealed other features that would be difficult to appreciate in tissue sections. First, the length of colon containing enteric neurons varied widely among pull-through resections (2–15 cm). This suggests some children might have done well with shorter resections if ENS could be visualized before or during pull-through surgery. This hypothesis is highlighted by the observation that HSCR11 had an additional 23.5 cm of proximal colon resected even though neurons were abundant in the proximal margin of the colon we received.

Second, density of myenteric neurons differed markedly over short distances for some children. For example, for HSCR4, a region 4 cm from the proximal resection margin had 1150 neurons/mm^2, whereas a region 2.3 cm more distal had only 42 neurons/mm^2. Similarly, for HSCR2, neuron density was 426 neurons/mm^2 at 3.5 cm from the proximal resection margin and only 17 neurons/mm^2 in a region 1.5 cm more distal. Abrupt changes in neuron density like this might explain why HSCR13 had no neurons at the proximal neomargin we analyzed, because clinical pathology retained the true proximal margin that contained myenteric and submucosal neurons in ∼80% of HSCR13's sampled circumference. Interestingly, HSCR13 was admitted for enterocolitis 6 months after pull-through surgery.

Third, submucosal and myenteric neuron density may differ markedly for defined transition zone regions. In 2 of our resections (HSCR2 and HSCR9), we found myenteric neurons in the distal colon that lacked submucosal neurons and 1 child (HSCR4) had submucosal neurons in a distal region with nearly absent myenteric neurons. Consistent with our results, analysis by other investigators of circumferential HSCR sections showed myenteric neurons up to 2 cm distal to submucosal neurons in 19 of 59 children and submucosal neurons distal to the myenteric plexus in 1 of 59.[17] These observations confirm the value of looking for submucosal and myenteric neurons when evaluating for ganglion cells.

Finally, in 3 children (HSCR2, HSCR7, and HSCR9), we found small patches of myenteric neurons in otherwise aganglionic bowel. Sections through these regions might be interpreted as "ganglion cells present," leading to retained aganglionic bowel. Collectively, these data suggest that whole-mount imaging could provide substantial insight into HSCR symptoms after pull-through surgery.

Limitations

It would be valuable to have data from more pediatric organ donor colons to define variability in ENS structure in children with normal ENS anatomy. Pediatric donor colon specimens were rare during our period of tissue collection, but we avoided analyzing colon from children with significant medical problems (eg, anorectal malformation) because this tissue may not be normal.

We also need to define in more detail how ENS structure varies along the length of the bowel. For example, our adult surgical biopsy specimens were all from the "distal colon," but we do not know whether they were from the descending or sigmoid colon. In addition, current data sets do not allow us to correlate anatomy with postsurgical outcomes, which will require a larger set of HSCR specimens.

Finally, although our approach is technically simple and reproducible, it cannot be used intraoperatively because staining takes 3 weeks and manual counting is time consuming. Our approach could be applied if HSCR surgery were performed in 2 stages (ie, initial ostomy, followed months later by pull-through surgery), but it would be ideal to have methods to visualize ENS anatomy in 3 dimensions while in the operating room. Confocal laser endomicroscopy or other new methods might solve this problem[18] if anatomic features predicting good outcomes could be unambiguously defined.

Conclusion

Managing HSCR and other disorders of the enteric nervous system can be very challenging, and current clinical pathology provides limited insight into ENS anatomy. Our new strategy evaluating the transition zone in HSCR without sectioning provides much more information about ENS structure. We hope that this approach can be leveraged to improve outcomes in HSCR and other bowel motility disorders.

Supplementary Material

Note: To access the supplementary material accompanying this article, visit the online version of *Gastroenterology* at www.gastrojournal.org, and at https://doi.org/10.1053/j.gastro.2024.02.045.

References

1. Swenson O, Rheinlander HF, Diamond I. Hirschsprung's disease: a new concept of the etiology. N Engl J Med 1949;241:551–556.
2. Marty TL, Seo T, Matlak ME, et al. Gastrointestinal function after surgical correction of Hirschsprung's disease: long-term follow-up in 135 patients. J Pediatr Surg 1995;30:655–658.
3. Polley TZ, Coran AG, Wesley JR. A Ten-year experience with ninety-two cases of Hirschsprung's disease including sixty-seven consecutive endorectal pull-through procedures. Ann Surg 1985;202:349–354.
4. Swaminathan M, Kapur RP. Counting myenteric ganglion cells in histologic sections: an empirical approach. Hum Pathol 2010;41:1097–1108.
5. Graham KD, López SH, Sengupta R, et al. Robust, 3-dimensional visualization of human colon enteric nervous system without tissue sectioning. Gastroenterology 2020;158:2221–2235.e5.
6. Heuckeroth R, Huerta Lopez S, Graham K, et al. Human colon tissue clearing and immunohistochemistry. Protocols.io. Available at: https://doi.org/10.17504/protocols.io.wyeffte. Published online February 21, 2020.
7. Furness JB. Types of neurons in the enteric nervous system. J Auton Nerv Syst 2000;81:87–96.

8. El-Salhy M, Sandström O, Holmlund F. Age-induced changes in the enteric nervous system in the mouse. Mech Ageing Dev 1999;107:93–103.
9. Knowles CH, Veress B, Kapur RP, et al. Quantitation of cellular components of the enteric nervous system in the normal human gastrointestinal tract—report on behalf of the Gastro 2009 International Working Group. Neurogastroenterol Motil 2011;23:115–124.
10. Dariel A, Grynberg L, Auger M, et al. Analysis of enteric nervous system and intestinal epithelial barrier to predict complications in Hirschsprung's disease. Sci Rep 2020; 10:21725.
11. Hanani M, Fellig Y, Udassin R, et al. Age-related changes in the morphology of the myenteric plexus of the human colon. Aut Neurosci 2004;113:71–78.
12. Parathan P, Wang Y, Leembruggen AJ, et al. The enteric nervous system undergoes significant chemical and synaptic maturation during adolescence in mice. Dev Biol 2020;458:75–87.
13. Schäfer K-H, Hänsgen A, Mestres P. Morphological changes of the myenteric plexus during early postnatal development of the rat. Anat Rec 1999;256:20–28.
14. Wester T, O'Briain DS, Puri P. Notable postnatal alterations in the myenteric plexus of normal human bowel. Gut 1999;44:666–674.
15. Wells TR, Landing BH, Ariel I, Nadorra R, Garcia C. Normal anatomy of the myenteric plexus of infants and children. Demonstration by flat-mount (circuit diagram) preparations. Perspect Pediatr Pathol 1987;11: 152–174.
16. Nestor-Kalinoski A, Smith-Edwards KM, Meerschaert K, et al. Unique neural circuit connectivity of mouse proximal, middle, and distal colon defines regional colonic motor patterns. Cell Mol Gastroenterol Hepatol 2022; 13:309–337.e3.
17. Kapur RP. Histology of the transition zone in Hirschsprung disease. Am J Surg Pathol 2016;40:1637–1646.
18. Shimojima N, Kobayashi M, Kamba S, et al. Visualization of the human enteric nervous system by confocal laser endomicroscopy in Hirschsprung's disease: an alternative to intraoperative histopathological diagnosis? Neurogastroenterol Motil 2020;32:1–8.

Received December 7, 2022. Accepted February 18, 2024.

Correspondence
Address correspondence to: Robert O. Heuckeroth, MD, PhD, The Children's Hospital of Philadelphia Research Institute, 3615 Civic Center Boulevard, Abramson Research Center, Suite 1116I, Philadelphia, Pennsylvania 19104-4318. e-mail: HeuckerothR@chop.edu.

Acknowledgments
The authors thank the families who participated in this study and their colleagues in Pediatric Surgery and Pathology at Children's Hospital of Philadelphia.

CRediT Authorship Contributions
Joshua D. Eisenberg, MD (Conceptualization: Equal; Data curation: Lead; Formal analysis: Lead; Investigation: Lead; Methodology: Equal; Validation: Lead; Visualization: Lead; Writing – original draft: Equal; Writing – review & editing: Equal)

Rebecca P. Bradley, BS (Data curation: Supporting; Formal analysis: Supporting; Investigation: Supporting; Validation: Supporting; Visualization: Supporting; Writing – review & editing: Supporting)

Kahleb D. Graham, MD (Conceptualization: Supporting; Investigation: Supporting; Methodology: Supporting; Writing – review & editing: Supporting)

Rachel H. Ceron, BS (Investigation: Supporting; Writing – review & editing: Supporting)

Amanda M. Lemke, MS (Investigation: Supporting; Writing – review & editing: Supporting)

Benjamin J. Wilkins, MD, PhD (Investigation: Supporting; Writing – review & editing: Supporting)

Ali Naji, MD, PhD (Investigation: Supporting; Writing – review & editing: Supporting)

Robert O. Heuckeroth, MD, PhD (Conceptualization: Equal; Data curation: Supporting; Formal analysis: Equal; Funding acquisition: Lead; Investigation: Equal; Methodology: Equal; Project administration: Lead; Resources: Lead; Supervision: Lead; Validation: Equal; Visualization: Supporting; Writing – original draft: Equal; Writing – review & editing: Equal)

Conflicts of interest
The authors disclose no conflicts.

Funding
This work is supported by the Suzi and Scott Lustgarten Endowment (Robert O. Heuckeroth), the Irma and Norman Braman Endowment (Robert O. Heuckeroth), Children's Hospital of Philadelphia Research Institute (Robert O. Heuckeroth), Children's Hospital of Philadelphia Frontier Program Center for Precision Diagnosis and Therapy for Pediatric Motility Disorders (Robert O. Heuckeroth), National Institutes of Health, National Institute of Diabetes and Digestive and Kidney Diseases grant T32 DK101371 (Joshua D. Eisenberg), and Human Pancreas Analysis Program (https://hpap.pmacs.upenn.edu/), part of Human Islet Research Network (RRID:SCR_014393; https://hirnetwork.org), and National Institute of Diabetes and Digestive and Kidney Diseases grant UC4 DK112217 (Ali Naji).

Data Availability
All supplementary videos and Z-stack image files will be made available via the SPARC Data Portal (https://sparc.science/). The direct link to access the videos and images will be provided by the corresponding author upon request.